11

Tailored Polymer Additives for Wax (Paraffin) Crystal Control

Aurel Radulescu[1], Lewis J. Fetters[2] and Dieter Richter[1]
[1]*Forschungszentrum Jülich GmbH, Jülich Centre for Neutron Science*
[2]*Cornell University, School of Chemical and Biomolecular Engineering*
[1]*Germany*
[2]*USA*

1. Introduction

Crude oils and refined middle distillate products such as diesel fuels, kerosene (jet fuel) or heating oil contain an important fraction of paraffins (alkanes) of high energy content with a broad linear (*n*-paraffins) and branched chain length distribution (Fig.1).

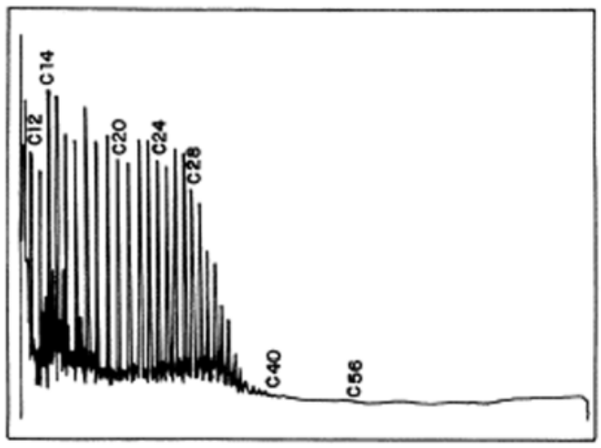

Fig. 1. Gas chromatogram of a virgin crude oil (del Carmen Garcia et al., 2000).

Depending on the type of crude deposits and refined technology applied, this fraction can vary between 10 and 30% (Coutinho et al., 2000). Although they are energetically desirable because of their increased combustion enthalpy with respect to C_5-C_{17} alkanes, the long chain C_{18}-C_{40} *n*-paraffins (waxes) are technically embarrassing when (1) their concentration is too high, (2) crude oils are extracted from deep sea reservoirs and pipeline transported through cold regions or (3) diesel fuels are used during the winter time (Kern & Dassonville, 1992). In these conditions, such fluids undergo dramatic degradation of viscoelastic properties due to precipitation of waxes as a consequence of the temperature drop and reduction of their solubility.

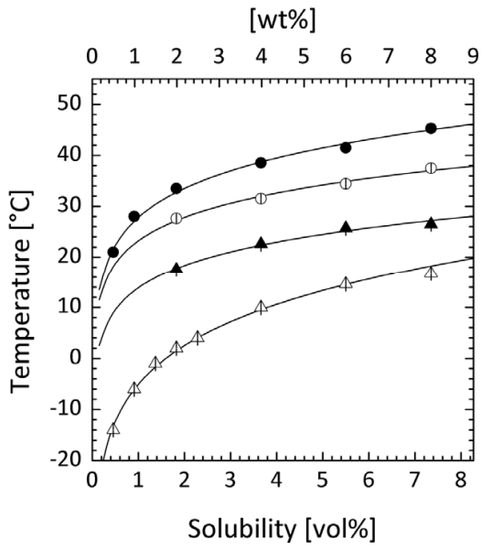

Fig. 2. Observed solubility lines of C_{24}, C_{28}, C_{32} and C_{36} waxes (from bottom to top) in decane (Ashbaugh et al., 2002).

The solubility point of *n*-paraffins (Fig.2) decreases with the increase of the carbon number (Srivastava et al., 1997): the higher the solubility point the more difficult is to keep the wax from precipitating. Wax precipitation is especially problematic during the production phase when the drop in the pressure and temperature of crude oils and the loss of short paraffins (light ends) to the gas phase occur (Pedersen et al., 1991a, 1991b). The waxes form stacked lamellar crystals with sizes of hundreds of micrometers and an overall morphology resembling a "house-of-cards" (Abdallah et al., 2000) that readily entrains liquid oil, primarily through surface tension, and effectively forms an organic gel. The occurrence and deposition of such large wax crystals cause a reduction of the ease of flow of crude oils and a loss of fluidity and filterability of middle distillates (Venkatesan et al., 2005; Singh et al., 1999). Wax deposition affects the storage tanks and conduits (Fig.3).

The pour point (PP) – the temperature at which the system gels and becomes mechanically rigid, - is about 10°C for a typical untreated oil and may vary over a wide temperature range below 0°C in the case of untreated diesel fuels (Claudy et al., 1993). A parameter that directly correlates to the occurrence of low temperature technical problems caused by the wax crystals is the cold filter plugging point (CFPP). This parameter corresponds to the temperature when plugging occurs in a 45μm filter under standardized conditions. For an untreated diesel fuel the CFPP is normally a few degrees higher than the PP.

In order to circumvent these technical problems "pour-point depressants" are added (Giorgio & Kern, 1983; Beiny et al., 1990). Generally, depressants are copolymers consisting of crystalline and amorphous segments that have the capacity to self-assemble in solution without sedimentation even at temperature well below 0°C. They interact favourably with paraffins and moderate the wax crystals morphology so that crude oils and middle distillates remain fluid as their temperature passes through that of PP. The mechanisms by which these polymeric systems modify the wax crystal size and shape are however incompletely understood. As such, the synthesis and choice of additives for crude oils and diesel fuels are largely trial and error rather than based on scientific principles. Moreover,

tests to evaluate the effectiveness of wax crystal modifying polymers concern generally the bulk properties and take rarely into consideration flow, cooling rate and composition conditions. A good knowledge of the wax-polymer interaction mechanism at microscopic scale as a function of wax content and temperature variation assesses the ability of a polymeric system to control efficiently the wax crystallization in hydrocarbon solution and enables the tailoring of additives for specific oil and middle-distillate composition conditions. The wax-polymer interaction in solution yields complex aggregates whose morphology strongly depends on the precipitation temperatures of both components. Therefore, besides information on the oil and diesel fuel composition a good characterization of the polymer self-assembling behaviour in solution is a prerequisite condition for the start of a structural study of wax-polymer interaction.

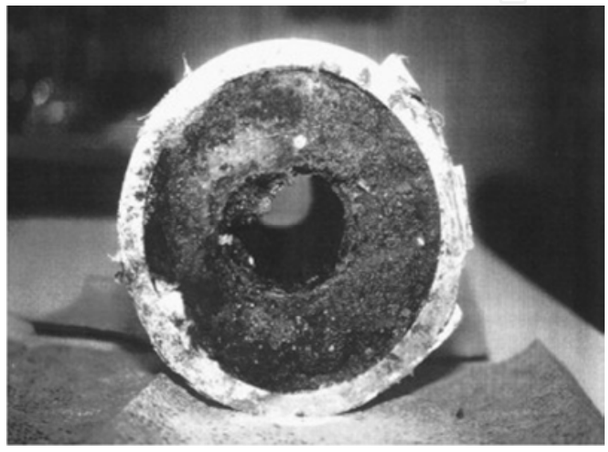

Fig. 3. Plugged pipeline (Banki et al., 2008).

Small-angle neutron scattering (SANS) technique exploiting on one side the strength of contrast matching and, on other side, the wide length scale explored, from 1nm up to 1μm, is a dedicated technique to investigate and elucidate complex morphologies such as those occurring in a wax-polymer-oil system (Richter et al., 1997; Leube et al., 2000; Monkenbusch et al., 2000; Schwahn et al., 2002a, 2002b; Ashbaugh et al, 2002; Radulescu et al., 2003, 2004, 2006, 2008, 2011). An eloquent example is that of diblock polymers (Fig. 4) of semi-crystalline polyethylene coupled to amorphous poly(ethylene-propylene) (PE-PEP) or poly(ethylene-butene) (PE-PEB) which yield in solution plate-like structures. The aggregates consist of a PE core shrouded behind an amorphous brush layer (Richter et al. 1997). The crystalline core serves as a nucleation platform for wax precipitation, while the amorphous brush acts as a steric barrier keeping the aggregates in solution. Rather than forming large platelets themselves, the waxes are sequestered by the diblock lamellar micelles (Leube et al. 2000). The elucidation of this wax modification mechanism by means of contrast matching SANS has found commercial application of PE-PEB (Infineum, Paraflow™) as diesel wax modifiers. More recently, following systematic SANS and optical microscopy studies, it was shown that the poly(ethylene-*co*-butene) random copolymers (Fig. 4), designated PEB-*n*, where *n* is the number of the ethyl side branches / 100 backbone carbons, could assume important oil and refinery applications because of their capability to modify the wax crystals precipitated at low temperature by model oil and diesel fluids (Ashbaugh et al., 2002; Schwahn et al, 2002b; Radulescu et al., 2004).

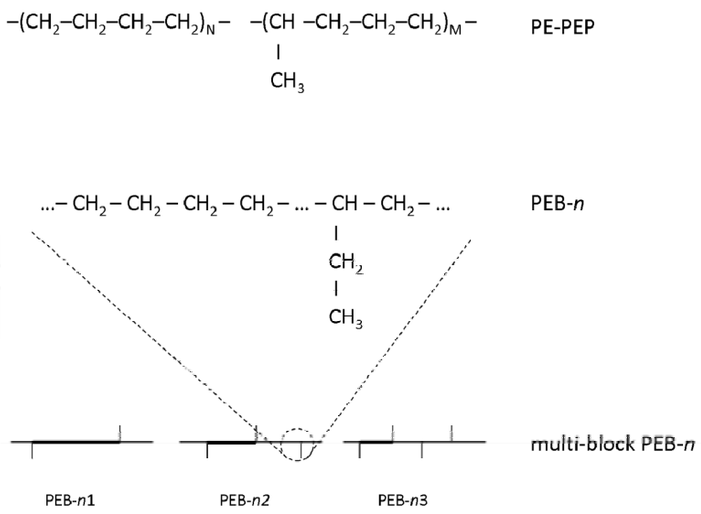

Fig. 4. Polymer structures designed and synthesized as efficient wax crystal modifiers following microstructural studies with SANS: crystalline-amorphous PE-PEP diblocks, semicrystalline PEB-*n* random copolymers with tuned crystallinity (variable number of ethyl side-groups*)* and multi-block PEB-*n* copolymers with graded crystallinity.

The studies on mixed hydrocarbon solutions of PEB-*n* copolymers and single paraffin waxes by contrast matching SANS revealed that these copolymers show selectivity in their wax modification capacity depending on the ethylene content of the backbones (Radulescu et al., 2003, 2004). The more crystalline copolymers show a higher efficiency for longer wax molecules while the less crystalline ones are very efficient for shorter waxes. This suggests that highly efficient PEB-*n* additives for crude oils and middle distillates should consist of segments with graded ethylene content. New polymers presenting variable crystallinity along the chain have been synthesized as multi-block copolymers built from segments representing PEB-*n* random polymers with blocks having different global content of ethyl branches (Fig.4). These new materials exhibit a gradual crystallization tendency of each block with decreasing temperature (Radulescu et al., 2011) which, considering the selectiveness of the PEB-*n* copolymers regarding their wax modification, tunes the crystallization behaviour of a broader distribution of wax molecules like those contained by crude oil and middle distillate fuel systems. In this case a gradual co-crystallization of those wax molecules and polymeric blocks presenting similar precipitation points eventually emerges. SANS and microscopy studies on polymer-wax solutions prepared for conditions closed to realistic ones, for high wax content or mixed wax molecules, have shown that such specifically designed polymers are able to template and control the wax crystallization in moderate size fluffy aggregates, thus arresting the growth of large compact waxy crystals and preventing the wax gelation which otherwise would eventually occur below 10°C.

2. Small-angle neutron scattering

Neutrons interact with matter via the short-range nuclear interactions and hence see the nuclei in a sample rather than the diffuse electrons cloud observed by X-rays. In magnetic samples neutrons are scattered by the magnetic moments associated with unpaired electron spins (dipoles). Unlike the X-rays, the neutrons are able to "see" light atoms in the presence

of heavier ones and to distinguish neighbouring elements more easily. Because the cross-section of an atom generally varies between isotopes of the same element, the exploitation of isotopic substitution methods can allow neutrons to highlight structural and dynamic details. Particularly, the strong difference in cross-section between hydrogen and deuterium enabling contrast variation methods is of a great importance for the investigation of synthetic organic compounds. Such complex structures spanning over a length scale from 1nm to 1 μm, can be characterized by SANS method.

2.1 SANS instruments and method

Elastic scattering with neutrons reveals structural information on the arrangement of atoms and magnetic moments in condensed matter systems. The information in such scattering experiments is contained in the neutron intensity measured as a function of the momentum transfer Q

$$\vec{Q} = \vec{k}_i - \vec{k}_f; \quad Q = \frac{4\pi}{\lambda} \sin\theta / 2 \tag{1}$$

where $\vec{k}_i$ and $\vec{k}_f$ are the incoming and outgoing neutron wave vector, λ is the neutron wavelength and θ is the scattering angle (Fig.5). Scattering experiments explore matter in reciprocal space and Q acts as a kind of inverse yardstick: large Q values relate to short distances, while a small Q relates to large objects. Aiming for the mesoscopic scale, SANS is optimized for the observation of small scattering angles using long wavelength (cold) neutrons. Thus, large objects, such as macromolecules, colloids, self-assembled systems, membranes, proteins, polymeric and biomolecular aggregates, etc., can be studied.

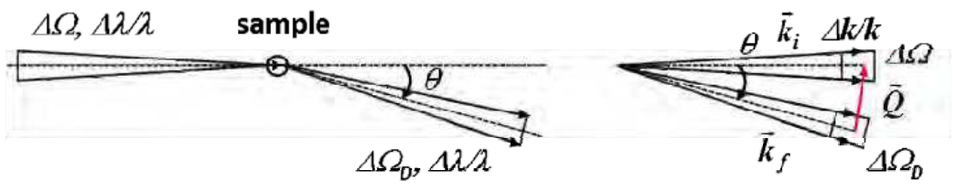

Fig. 5. Scattering process in real (left) and reciprocal (right) space; the divergence of the primary beam is described by the space angle $\Delta\Omega$, while the scattered intensity is measured in a detector element with space angle $\Delta\Omega_D$.

The principle layout of a conventional pinhole SANS instrument is shown in Fig.6. The high intensity requests in the case of SANS can only be achieved by using a large wavelength distribution of the monochromatic beam delivered by the mechanical velocity selector, typically $\Delta\lambda/\lambda$=10%-20%. A resolution-optimized setting of a SANS instrument is achieved if the collimation length L_C equals the sample-to-detector distance L_D. Therefore, the geometrically optimized SANS instruments have a typical length of 40m, reaching 80m for D11 at the ILL, Grenoble. Using neutron wavelengths between 4.5 and 20Å the Q interval between $7x10^{-4}$Å^{-1} and 0.5Å^{-1} becomes accessible in the classical pinhole mode.

In order to increase further the Q resolution towards smaller values, focusing optical elements need to be introduced. One possibility are the refractive optical elements – neutron lenses, placed in front of the sample such that a small incoming neutron beam is focused on

the detector and thus, smaller scattering angles than for conventional pinhole geometry are accessed (Frielinghaus et al., 2009).

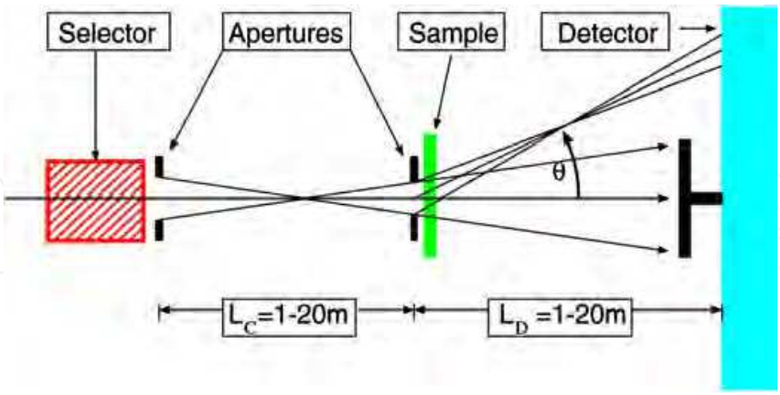

Fig. 6. Principle of pinhole SANS; a neutron beam entering the instrument from the left is the subject of monochromation (done by the velocity selector), collimation over a variable distance (achieved by using a set of adaptive system of apertures), scattering on the sample and detection on a two-dimensional position sensitive detector over long distances; aiming for detecting neutrons at small scattering angles the SANS instruments are very long.

Focusing-SANS using reflective (mirror) systems (Alefeld et al., 2000) was in use since longer time at the KWS-3 instrument operational at the FRM II reactor, Garching-München. In such an instrument the monochromated neutrons enter through a small aperture (typically 1mm) and hit the focusing mirror with the full divergence provided by the neutron guide. The mirror reflects and focuses the neutron beam on a high-resolution position sensitive detector (0.5mm space resolution) placed in the focal plane. The sample position is placed just after the mirror. Both focusing methods extend the pinhole SANS Q-range down to $1x10^{-4}Å^{-1}$.

SANS is thus a well-established, non-destructive method to examine structure on length scales of 1nm to 1μm.

2.2 SANS cross-section of simple structures

A crucial feature of SANS that makes it particularly useful for synthetic organic macromolecules (soft matter) is the ability to vary the scattering contrasts between different constituents of a hydrocarbon sample over a broad range by H/D substitution. Since the molecules affected by H/D exchange are chemically the same, the physical chemistry of the sample is only marginally modified, if at all. The visibility of an object M in solution S for example depends on the difference of the solvent/solute scattering length densities:

$$\Delta\rho_M = \left(\rho_M - \rho_S\right) = \frac{\sum_{i}^{atoms\ in\ M} b_i^M}{\nu_M} - \frac{\sum_{j}^{atoms\ in\ S} b_j^S}{\nu_S} \tag{2}$$

where b_i^M denotes the scattering length of the different atoms in M and b_j^S those of the atoms in S, while ν_M and ν_S are the effective volumes occupied by the objects composed of

the atoms in the respective sums. Since b_H = -3.57x10^{-13} cm, b_D = +6.57x10^{-13} cm and b_C = +6.65x10^{-13} cm, H/D replacement allows for huge variation of $\Delta\rho$ for hydrocarbons. Using a mixture of suitable amounts of deuterated and protonated solvent in general it is possible to achieve "zero contrast" $\Delta\rho = 0$ for one component of the system (Fig.7). The technique of contrast variation allows for highlighting parts of a structure and is of essential importance for the investigation of complex multi-component systems. The exchange of hydrogen with deuterium either in the solvent or explicitly in chemical groups of the organic macromolecules of interest (labeling) is then required. Deuterium labeling of synthetic organic macromolecules (polymers) is easily achieved by special synthesis methods.

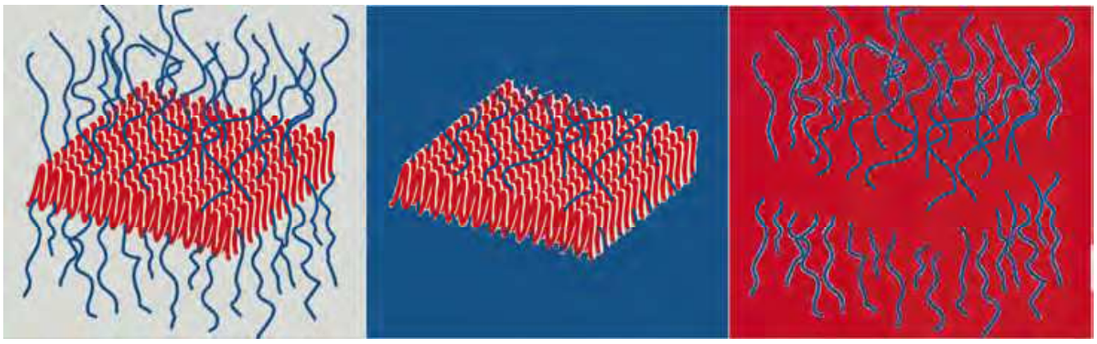

Fig. 7. Example of contrast matching between different domains of a diblock copolymer two-dimensional micelle (crystalline-amorphous core-brush morphology) and solvent: by modification of the solvent scattering length density the full contrast, core contrast and brush contrast (from left to right) can be adjusted.

The contribution to the small angle scattering intensity from some object is contained in the macroscopic cross-section $d\Sigma/d\Omega(Q)$, which is the absolute square of the Fourier transform of its scattering length density distribution $\Delta\rho(\vec{r})$ normalized by the sample volume V_{sample}. In case of N identical particles of volume V_p which are located at random positions and random orientations in a solution (with $N\,V_p = \phi\,V_{sample}$, where ϕ is the volume fraction of the scattering particles in solution) and are homogeneously decorated with a constant contrast factor $\Delta\rho$, the macroscopic scattering cross-section can be written as

$$\frac{d\Sigma}{d\Omega}(Q) = \frac{N}{V_{sample}} \Delta\rho^2\, V_p^2 P(Q)\, S(Q) \tag{3}$$

where $P(Q)$ represents the particle form factor, which relates to intra-particle correlations, and $S(Q)$ the structure factor, which denotes the inter-particle correlation effects. The analysis of the form factor $P(Q)$ and structure factor $S(Q)$ in terms of structural models (Pedersen, 1997) delivers information about the size, shape, number density, and correlation between the scattering particles in the sample. The evaluation of the "forward scattering" $d\Sigma/d\Omega(Q\rightarrow 0)$, which amounts to $\phi\,\Delta\rho^2 V_p$, offers information about the volume fraction of the scattering particles while knowing the contrast from the synthesis procedure and the size of the scattering objects from the scattering data.

For multi-component systems containing for example, oil, polymer and wax, the scattering cross-section in terms of the partial scattering functions assumes the form:

$$\frac{d\Sigma}{d\Omega}(Q) = (\rho_P - \rho_S)^2 P_{PP}(Q) + 2(\rho_P - \rho_S)(\rho_W - \rho_S) P_{PW}(Q) + (\rho_W - \rho_S)^2 P_{WW}(Q) \tag{4}$$

where the indexes P and W indicate the polymer and wax, respectively. If the scattering length density of the single components is changed within given limits by hydrogenation or deuteration, either the polymer (ρ_W=ρ_S) or the wax (ρ_P=ρ_S) can be left visible in the sample.

The wax and semicrystalline polymer molecules yield in solution complex morphologies displaying multiple structural levels that are sometime hierarchically organized on a scale from nanometers to hundreds of microns. Basically, these morphologies evolve from lamellar or rod structural units. Depending on the polymer architecture, a crystalline-amorphous morphology emerges in solution either as core-brush lamellae or as density modulated rods. For a core-brush two-dimensional morphology formed by diblock copolymers in solution (Richter et al., 1997) the cross section is expressed as

$$\frac{d\Sigma}{d\Omega}(Q) = \phi \frac{\nu_c}{V_c} P(Q)\left(\pi R^2\right)^2 \frac{D(QR/2)}{(QR/2)} + I_{blob} \tag{5}$$

Thereby, ϕ is the volume fraction of polymer in solution (as aggregates), ν_C is the fraction of the crystallizable segment in the polymer, R is the lateral dimension of the lamellae (discs) and $D(x)$ denotes the Dawson function. The second term in Eq.5 arises from the polymeric structure of the brush (the "blob" scattering). $P(Q)$ is the form factor of the density profile perpendicular to the lamellae surface including the contrast factors of the core and the brush parts and the density profiles of the polymer volume fraction. The form factor of an infinitely large plate of the thickness d considering a simple rectangular density profile is

$$P(Q) = \left[\sin(Qd/2)/(Qd/2)\right]^2 \tag{6}$$

For the amorphous brush different approaches can be adopted varying from a simple rectangular profile to a parabolic or even a more complicated prediction. When the platelets stack the structure factor of one-dimensional paracrystalline order can be used, which in the case of an infinite stack has the form

$$S(Q) = \frac{\sinh\left(Q^2\sigma_D^2/4\right)}{\cosh\left(Q^2\sigma_D^2/4\right) - \cos(QD)} \tag{7}$$

where D is the stacking period and σ_D is its Gaussian smearing.

The form factor appropriate for an ensemble of isotropic oriented homogeneous rods of thickness a and very large length $2H$ can be expressed, for the condition $Q>>\pi H$, $H>>a$, as

$$P(Q) = \frac{\pi}{Q\,2H}\left[\frac{2J_1(Qa)}{(Qa)}\right]^2 \tag{8}$$

where $J_1(x)$ is the first order Bessel function of the first type. More complicated equations requiring numerical calculations are involved for inhomogeneous rods (Radulescu et al., 2004) or for rods with elliptical cross-section (Bergström & Pedersen, 1999).

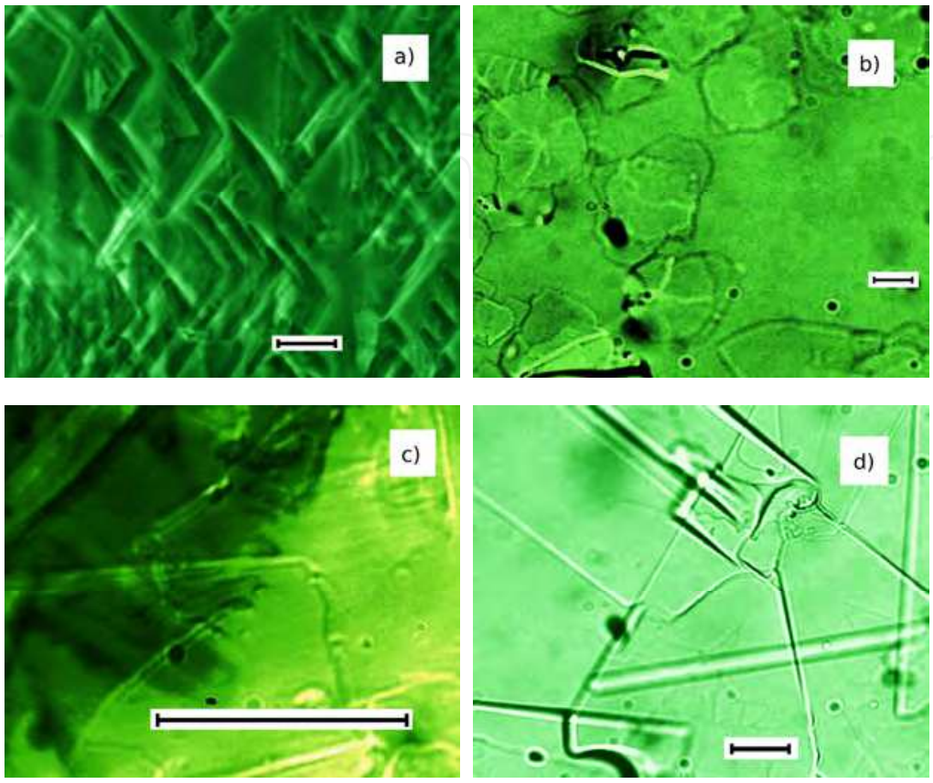

Fig. 8. Micrographs from decane solutions of mixed 1%C_{36}/1%C_{30} at 0°C (a), 0.5%C_{24} at -20°C (b), 1%C_{36} at 20°C (c) and 4%C_{24} at -10°C (d); scale bars 30μm.

The combination of scattering data with fractal geometry concepts recently commenced to become a general path of investigating the complex morphologies displaying multiple structural levels on wide length scales (Beaucage & Schaefer, 1994). Fractal approaches describe power-law regimes often observed in measured scattering profiles with the exponents depending on the geometric structure of the scattering objects, $d\Sigma/d\Omega(Q) \approx Q^{-p}$. If the mass of an object scales with its size according to $M \approx R^D$, one deals with the mass fractals that can be simply characterized by the exponent D, the mass fractal dimension. The scattering cross-section from mass-fractal objects is proportional with Q^{-D} and thus, a power law regime in Q with an exponent $p=D=1$ relates to rod-like structures, $p=D=2$ to platelets and $p=D=3$ to uniformly dense structures. Surface fractals are uniformly dense objects presenting a fractally rough surface that scales with their radius $S \approx r^{Ds}$, where D_S can assume values between 2 (smooth surface) and 3 (extreme roughness). For fractally rough surfaces, the power law exponent becomes $p=D_S-6$ and, if the object possesses a smooth surface, $p=4$ (Porod scattering), while for a rough surface $3 \leq p \leq 4$. Empirically, one may also find slopes steeper than those corresponding to $p=4$. In this case, the objects have diffuse rather than fractally rough interfaces. An observed structural level and its associated power-law for simple well defined shape objects can be analyzed using the graphical presentation

of data in terms of Guinier approximation, $\ln(Q^p\, d\Sigma/d\Omega)$ vs. Q^2, which delivers in a direct way the "forward scattering" and the size of the objects (Schwahn et al., 2002a).

3. Wax crystallization from hydrocarbon solution

Below the solubility line (Fig.2) wax precipitates in large crystals. Depending on solution conditions, such as molecule length, wax concentration, temperature, or whether there is a single- or multi-wax solution, the crystal morphology varies to a large extent (Fig.8). Isolated well-defined lozenge-shaped pyramidal plates (Fig.8a), flat conical objects with irregular edges (Fig.8b) or "house-of-cards" morphologies of compact crystals (Fig.8c,d) are observed.

Such large crystals with sizes between several and hundreds of microns provide a strong small-angle scattered intensity (Fig.9). Although in all conditions large crystals are formed the profiles differ significantly and relate to the asymptotic power-law scattering behaviour typical of the differing morphologies formed. The size of the crystals finds itself within micrometer range, i.e. the typical features from such large morphologies appear within very low Q domains, well out of the measured range by classical pinhole SANS. The power-law indicates formation of three-dimensional fractal-like structures having an extremely rough surface (p=3) as in the case of short chain waxes at low content or those where p=4 (typical for high wax contents or long waxes). Mixed wax crystals exhibit surface fractal features.

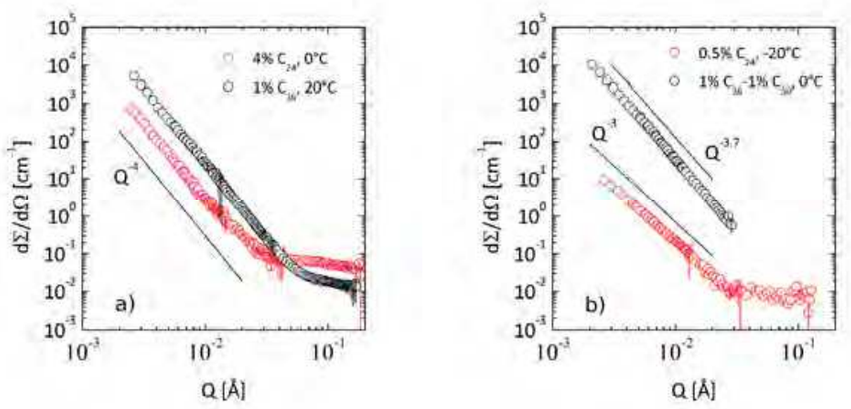

Fig. 9. SANS traces from solutions of different waxes in decane.

4. Crystalline-amorphous PE-PEP diblock copolymers

The crystalline-amorphous poly(ethylene)-poly(ethylene-propylene) (PE-PEP) diblock copolymers yield in decane platelet-like aggregates (Richter et al., 1997; Leube et al., 2000). Such a morphology is adopted as a consequence of the crystallization of the PE-blocks in thin lamellar crystallites (d≈20-50Å), whereas the PEP forms brushes on both sides of the lamellae. Unlike the lower molecular weight M_W compounds that yield isolated platelets, the higher molecular weight copolymers form larger platelets showing stacking tendencies due to mutual van der Waals attraction acting on the large surface area. SANS investigations were performed in order to quantitatively understand the aggregation phenomena occurring in solution and to decipher the influence of PE-PEP additives on the wax crystals

formed at low temperatures in common hydrocarbon solutions. Empirically, the PE-PEP diblock systems have proven to exhibit wax crystal modification activity in various diesel fuels. Whether a co-crystallization of wax molecules with the PE-block in the core or another wax-polymer interaction mechanism takes place, was the fundamental question addressed by SANS. For this purpose, a series of well-defined diblocks with different PE-PEP compositions and molecular weights was synthesized by anionic polymerization of polydienes followed by the saturation of the resulting polymer by hydrogenation. This is a convenient method in the case where well-define molecular weights and structures are needed. In a first step polybutadiene-polyisoprene (PB-PI) diblocks were obtained by polymerization of 1,3-butadiene and 2-methyl-1,3-butadiene in nonpolar hexane. The M_W was characterized by low-angle laser-light scattering and by size exclusion chromatography. The thus synthesized polymers were in a second step saturated by hydrogenation or deuteration at 80-100°C under a pressure of 25-30 bar using palladium on barium sulphate as a catalyst. Due to the occasional occurrence of 1,2-addition of butadiene the PE chains in the final polymer contain about 2 ethyl side branches/100 backbone carbons.

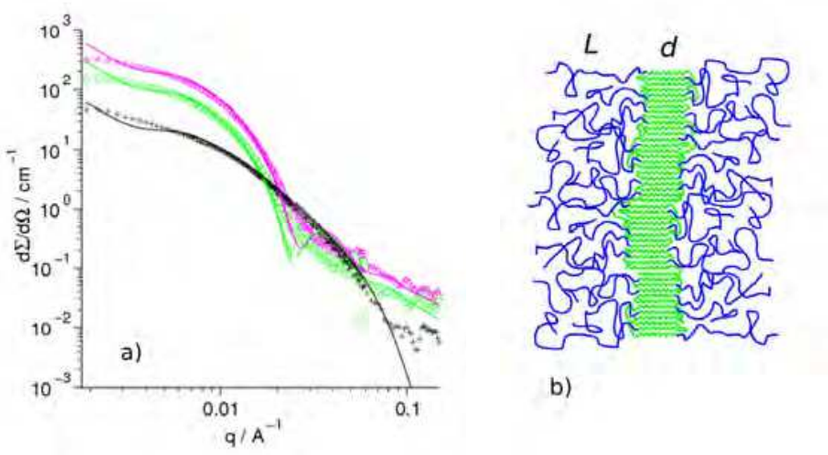

Fig. 10. (a) Example of scattering patterns from PE(1.5kg mol^{-1})-PEP(5kg mol^{-1}) diblock in decane for the common (green), core (black) and brush (pink) contrast conditions (Leube et al., 2000). The solid lines denote the simultaneous fit of the data according to the two-dimensional core-brush model (Eq.5) including a rectangular core profile and a parabolic brush profile; (b) Sketch depicting the PE-PEP structure in solution as emerged from the model interpretation of the SANS data, with L the brush length and d the core thickness.

To utilize the full capabilities of SANS the contrast was controlled by the variation of the scattering properties of different polymer components by varying the degree of hydrogenation and deuteration in the precursor PB-PI block copolymers and/or during the saturation. Furthermore the wax was contrasted out or made visible depending on the degree of hydrogenation and deuteration of the different components.

Fig.10a presents the scattering data from a low M_W PE-PEP copolymer in decane (ϕ_{pol}=2%) at room temperature for different contrast conditions enabled by the variation of the solvent scattering length density in equal steps between fully deuterated decane (ρ_S=6.2 x 10^{10} cm^{-2}) and fully protonated decane (ρ_S=-0.3 x 10^{10} cm^{-2}). Detailed measurements were performed on decane solutions of largely different M_W copolymers by varying the polymer volume

fraction in solution and the scattering length density of polymer blocks and solvent. The fit of such data using Eq.5 with different profiles for the core and the brush morphologies delivered the platelet thickness d and the brush length L, both parameters which vary with M_W. Taking into consideration the structural features revealed by SANS and the thermodynamic aspects of the platelets formation (core thickness and brush length adjust themselves from a balance between the entropy loss in the stretched brush on the one hand and the enthalpy costs of folding the polyethylene chains and defect energies associated with the incorporation of ethyl side branches on the other hand) the structure of the PE-PEP aggregates (Fig. 10b) consisting of a thin crystalline core exhibiting a certain surface roughness and a stretched amorphous brush was fully characterized and understood.

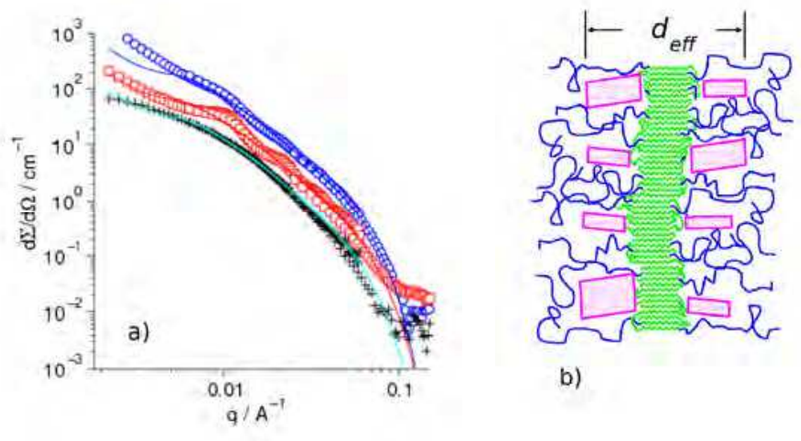

Fig. 11. (a) Example of scattering from PE(1.5 kg mol^{-1})-PEP(5 kg mol^{-1}) with no wax (black), 0.5% C_{36} (blue) and 0.5% C_{30} (red) added, under common core and wax contrast, at 5°C (Leube et al., 2000): the scattering patterns follow a Q^{-2} behaviour; (b) Sketch depicting wax crystallites (pink) nucleated at the crystalline PE core and sequestered by the PEP brush.

The effect of wax on the scattering from diblocks was studied in different contrast conditions (Leube et al., 2000), which allowed the core, the brush or commonly the core and wax visible. A comparative analysis of the polymer core and brush scattering profiles for neat and C_{36} hexatriacontane wax-dopped polymer solutions in decane offered the first insight about the changes occurring at the level of polymer morphology in the presence of wax. The results revealed no change of scattering for core contrast, thus no change in the core thickness, while the brush density profile was found to be shifted outward in the presence of wax compared to the polymer self-assembling case, which indicates more stretched hairs close to the core surface. These findings prove that there is no incorporation of wax into the core. Apparently, the wax enters the brush probably by a nucleation and growth on top of the core. SANS investigations under common core and wax contrast condition revealed an increase in thickness of the two-dimensional aggregates, i.e. the adsorbed crystallized wax enters through the brush and adds to the effective core thickness.

Following detailed contrast matching SANS investigation (Fig. 11a) the increase in the effective core thickness d_{eff} due to addition of wax crystallites was evaluated. Supposing an average surface coverage by wax, from the fit of the scattering patterns the crystallized wax volume fraction was obtained: for 0.5%C_{36} wax dissolved in the initial solution almost 100%

wax aggregation was found at 5°C, while in the case of 0.5%C_{30} solution the wax aggregation fraction is only 57%.

In conclusion, by means of the SANS micro-structural investigation method the structure and morphology of the crystalline-amorphous polymer-aggregates was resolved (Fig.11b). Of greater importance for further design and optimization of efficient polymer additives for wax crystal control was the understanding of the interaction mechanism between the polymers and waxes in this specific case. This mechanism has found commercial application of PE-PEB (Paraflow™) as diesel wax modifiers.

These crystalline-amorphous diblock copolymers are effective at breaking the wax gels at low wax concentration. In applications where the dissolved wax concentration is large, such as crude oils, wax precipitation can bury the PEP or PEB brush layers negating thus the steric stabilization advantages and grow ultimately in large crystals. Other more versatile crystalline–amorphous polymer architectures expressing a higher efficiency in controlling the wax crystallization at high wax content have been designed based on micro-structural information obtained by SANS.

5. Crystalline-amorphous poly(ethylene-butene) copolymers PEB-*n*

The behaviour of PE-PEP and PE-PEB diblock copolymers with respect to their ability to control the wax crystallization invited the evaluation of PEB-based copolymer architectures where semi-crystalline and amorphous segments are combined in an alternative or random manner. One such family is represented by nearly random copolymers of ethylene and 1-butene obtained by the anionic polymerization of butadiene with variable 1,2- and 1,4-modes of addition (Morton & Fetters, 1975). The microcrystallinity of these polymers designated PEB-*n*, where *n* is the number of ethyl side branches/100 backbone carbons, can be tuned by changing the ratio ethylene to butene segments, i.e. by varying *n*. Thus, PEB-0 represents essentially crystalline high density PE, while for n>13 crystallinity is absent in the bulk state. The reactivity ratio product obtained from the ^{13}C-NMR evaluation of the sequence distribution characteristics of PEB copolymers suggested their random character. The self-assembling features of PEB-*n* copolymers in decane solution were investigated by SANS. Following carefully observation of the scattering patterns with decreasing temperature it was found that the assembling events appear at a temperature which is the higher the lower *n* (Ashbaugh et al., 2002; Radulescu et al., 2003). Thus, PEB-7.5 shows first aggregation tracks already at 40°C while PEB-11 only at 0°C. Despite this difference the scattering cross-section of copolymers with different number of ethyl side groups shows at low temperature a well-defined Q^{-1} power-law profile which is indicative for rod like aggregates. Fig.12a displays example of SANS patterns from the PEB-7.5 (6kg mol^{-1}) aggregates at -10°C for different polymer volume fraction ϕ_{pol} in solution. (Radulescu et al., 2004). The length of the rods is not accessible by classical SANS since no saturation of scattered intensity towards low Q is observed. The peak-like structure appearing at the same Q position for different ϕ_{pol} denotes intra-particle correlations and arises from longitudinal modulation of the rod density. Following the interpretation of the experimental data by appropriate structural models the polymer rods were characterized with respect to their lateral size and density parameters and a self-assembling mechanism was proposed. The polymer volume fraction inside the rod structures with thickness of 50-60Å and modulation period of 300-350Å is low and could range between 4% and 20% depending on the actual volume fraction of rods in solution.

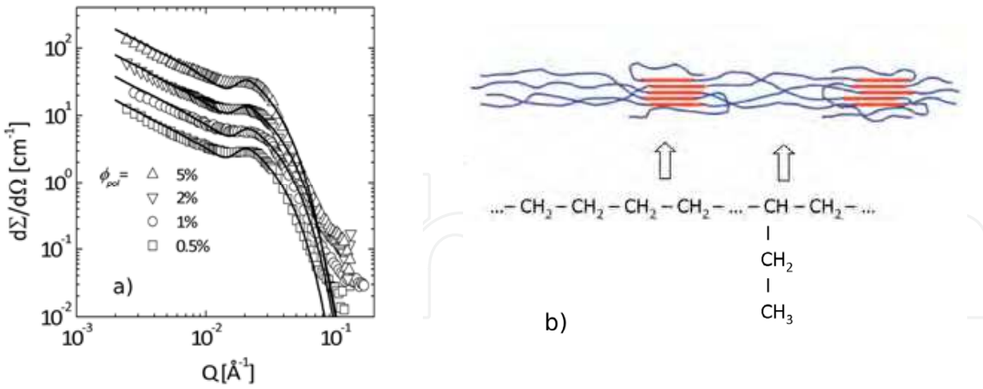

Fig. 12. (a) Examples of SANS patterns from PEB-7.5 copolymer in decane for different ϕ_{pol} at -10°C (Radulescu et al., 2004); (b) Sketch depicting the structure of PEB-*n* random copolymers in solution as emerged from the analysis of SANS data.

This finding shows that the polymer assemblies are solvent swollen open objects. Formation of such morphology was explained by taking into account the molecular architecture of the PEB-*n* random copolymers: the aggregation events occur as a consequence of crystallization of the longer PE sections within one chain while the amorphous sequences containing ethyl side groups form a loose corona around the crystalline nucleus and screen it against the intrusion of other chains by osmotic repulsion. The rarity of co-crystallization events promotes thus a one-dimensional growth (Fig. 12b). For PEB-*n* materials with lesser crystallinity an attenuated or "no peak" feature was noticed in the SANS patterns. That indicates a more homogeneous polymer density inside rods (Schwahn et al., 2002a).

The self-assembly behaviour of the PEB-*n* copolymers with variable crystallinity led to the conjecture that their interaction with waxes may depend on the correlation between the self-assembly temperature and the wax solubility point within the investigated range of wax concentration. The density of the ethyl side groups and the M_W may thus control the efficacy of different PEB-*n* copolymers in modifying the size and the shape of waxy crystals formed in decane. The understanding of their positive effect on the low-temperature viscoelastic properties of waxy fluids was possible following combined rheology, microscopy and SANS studies (Ashbaugh et al, 2002; Schwahn et al., 2002b; Radulescu et al., 2004, 2006). Fig.13a,b presents micrographs collected at different temperatures from decane solutions of 1% C_{36} and 4% C_{24} when 0.6% PEB-7.5 is added (Radulescu et al., 2004, 2006). Marked changes in the wax crystallization habits are observed in the presence of polymer compared with crystallization from pure solutions (Fig.8c,d): instead of big compact plates several hundreds of μm in size smaller morphologies exhibiting a soft texture or thin needles with modulated thickness appear in the presence of polymer.

The formation and hierarchical evolution of such morphologies with decreasing temperatures were characterized by SANS over a wide *Q*-range. Again, the use of contrast allows the identification of wax conformation and the polymer inside the common aggregates. This also aids in the understanding of the microscopic interaction mechanisms.

The assembly events depend on the length of the crystallizable segments that are either the wax molecule or the ethylene sections of the copolymer. Formation of multilevel hierarchical morphologies is a consequence of one component to crystallize prior to its companion and to template the final overall morphology. Conversely, for the case of well-matched self-assembling properties cooperative co-crystallization is allowed. Typical pinhole SANS results are shown in Fig.14a,b, which presents under polymer and wax contrast, respectively, scattering patterns from wax-polymer mixed solutions which are typical for the two mechanisms identified (Radulescu et al., 2003, 2004).

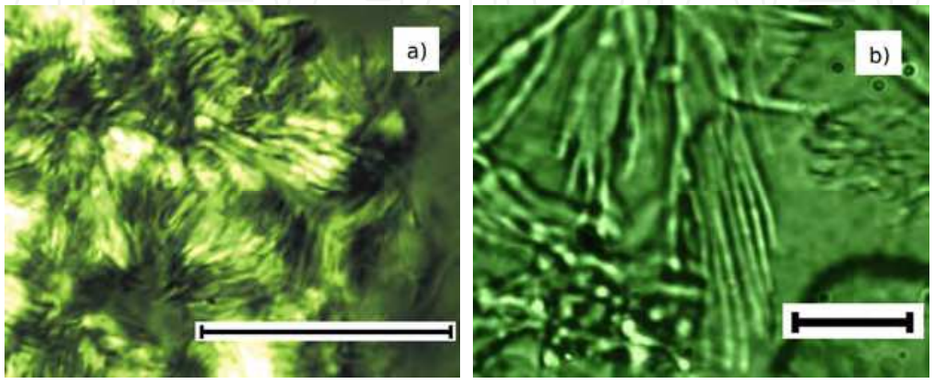

Fig. 13. Micrographs from PEB-7.5 doped decane solutions of 1%C_{36} at 20°C (a) and 4%C_{24} at -10°C (b); scale bars 30μm (Radulescu et al., 2004, 2006).

In the first example, when 0.6%PEB-7.5(6kg mol^{-1}) and 1%C_{24} are mixed in decane, the polymer commences self-assembling in its characteristic density-modulate rod-like structure well before the wax crystals appearance. At temperatures below the wax crystallization line the polymer and wax influences each other's aggregation behaviour (Fig.14a). On the one hand, the wax crystallization influences the polymer structure, which changes from rod-like (~Q^{-1}) to plate-like (~Q^{-2}) in the presence of wax. Thus, co-crystallization of the polymer and wax occurs below certain temperatures. On the other hand, the wax scattering patterns reveal the correlation peak at the same Q-position where it is observed for the polymer alone. Thus, it looks like in the case when polymer assemblies are formed at higher temperatures than the wax precipitation point the common aggregation habit is dictated by the primordial polymer structure which serves to template the subsequently formed wax-polymer plates in a shish-kebab-like correlated arrangement. This is demonstrated by the TEM observation of aggregates (Fig.15a) isolated at room temperature from a mixed decane solution of high M_W PEB-7.5 (30kg mol^{-1}) and C_{36}, a ternary system that exhibits at higher temperatures similar scattering features and experiences the same aggregation mechanism like the combination of low M_W PEB-7.5 and C_{24}. The simultaneous fit of the scattering data for different contrast conditions considering correlated wax layers embedded into thicker polymer platelets (Eq.5-7) delivered the geometrical and density parameters of the wax-copolymer aggregates. These consist basically of a single layer of stretched C_{24} molecules (d_{wax}=32Å) embedded into thicker polymer platelets (d_{pol}=100-150Å) which grow around the crystalline nuclei of initial polymer rods and are correlated over distances of D=200-230Å with a smearing of σ_D=100-140Å. This mechanism yields eventually a shish-kebab-like morphology (Fig.15a).

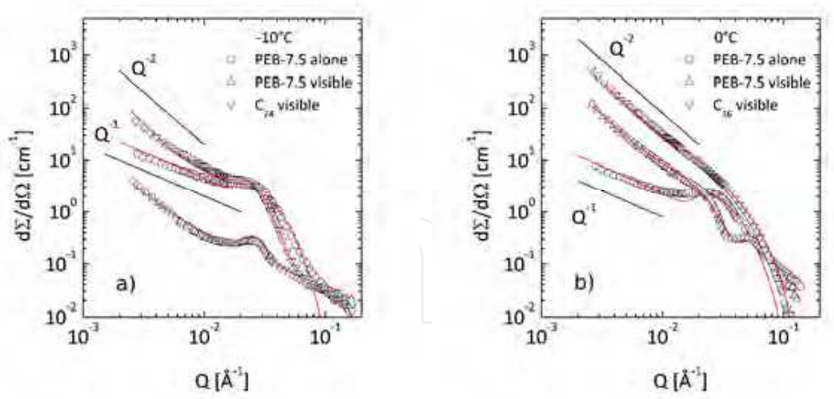

Fig. 14. Examples of wax and polymer SANS profiles (triangles) from PEB-*n*/wax mixed solutions in decane (Radulescu et al., 2004) for 0.6%PEB-7.5/1%C_{24} at -10°C (a) and 0.6%PEB-7.5/0.5%C_{36} at 0°C (b); the polymer self-assembling SANS patterns (circles) are shown in parallel in order to emphasize the structural changes induced by the addition of wax; the curves represent model description of the data (see text).

In the second example, when 0.6%PEB-7.5 (6kg mol^{-1}) and 0.5%C_{36} are mixed in decane, the wax and polymer show quite similar precipitation temperatures and yield extended joint polymer-wax plate-like structures which are loosely correlated due to van der Waals interaction. The co-crystallization of wax and copolymer in thin platelets is again the main mechanism that changes the polymer scattering pattern from ~Q^{-1} into ~Q^{-2} (Fig.14b). A homogeneously distributed polymer profile across well-defined platelets of narrow size distribution was deduced from the observation of the form factor features towards high Q. Again, the simultaneous fit of different contrast scattering patterns according to Eq.5-7 resulted in monolayer of stretched wax molecules embedded within a thicker polymer layer, a morphology which is depicted by Fig.15b.

From the quantitative analysis of the scattering profiles systematically collected over a wide temperature range for different wax-copolymer combinations and volume fractions it was concluded that the co-crystallization mechanism of wax and crystallizing segments of the copolymer emerging as a consequence of the good match between precipitation temperatures of both components corresponds to a high efficiency of the polymer in controlling the size and shape of the wax crystals. In this case, for ϕ_{wax}=0.5% in the initial solution about 80% stays inside polymer-wax common thin platelets at 0°C in the case of C_{36} combined with PEB-7.5(6kg mol^{-1}) and at -22°C in the case of C_{24} combined with PEB-11(6kg mol^{-1}). The amount of polymer contained by the aggregates is very small and corresponds to much less than a half of the volume fraction in the initial solution. The wax volume fraction inside the wax layer is about ϕ_{wax}=70-90%, while the polymer volume fraction inside the polymer layer is about ϕ_{pol}=10-30%. For higher wax contents, a considerable amount of wax is entrapped by the thin platelets, e.g. for ϕ_{wax}=2% C_{36} in the presence of PEB-7.5(6kg mol^{-1}) this amounts at 0°C to about 55%. A lower efficiency was observed in the case of wax crystallization templated by polymer one-dimensional morphologies pre-existing in solution: only a maximum of about 10-15% of ϕ_{wax}=0.5% C_{24} is contained by the correlated polymer-wax plates at -20°C for a corresponding 50% of the polymer consumed from the

amount in the initial solution. Lower wax volume fraction, about ϕ_{wax}=30-60% characterizes the wax layer, while the polymer volume fraction inside the polymer layer is about ϕ_{pol}=40-70%. It was shown that, in this case, later crystallization stages or the wax surplus (like for ϕ_{wax}=4%) led to thickening of the platelets anchored at the polymer density-modulated rod-like structures, which ultimately join together and give raise to formation of long needles with modulated thickness like those visible in Fig.13b.

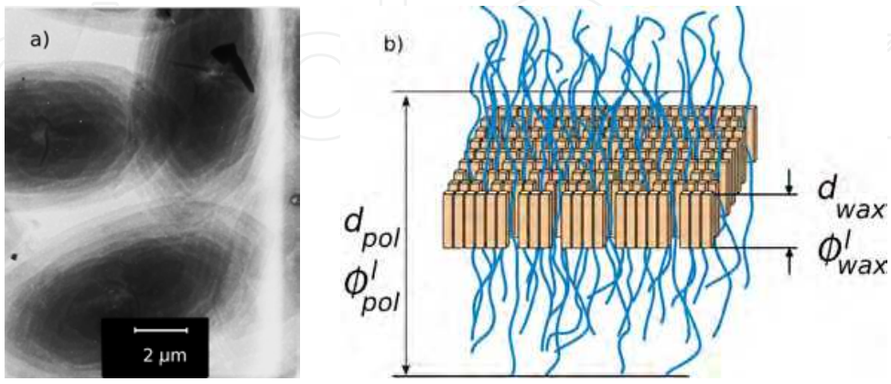

Fig. 15. (a) TEM image of wax-polymer correlated plates resembling a top view of a shish-kebab morphology; (b) Cartoon of the polymer-wax aggregate consisting of monolayer of stretched wax molecules embedded into thicker homogeneous polymer layer; the thickness and material volume fraction characterizing each layer are indicated (Radulescu et al., 2008).

From the micro-structural investigations of mixed solutions of PEB-*n* random copolymers and single waxes it emerges thus the conclusion that these polymers show selectivity in their wax modification capacity depending on the ethylene content of the backbones: the more crystalline copolymers show a higher efficiency for longer wax molecules, whereas the less crystalline ones are very efficient for shorter waxes. This basic result directly suggested that highly active PEB-*n* additives for crude oils and middle distillates should consist of segments with graded ethylene content.

6. Multi-block PEB-*n* copolymers

Two PEB-*n* multi-block copolymers, a tetra-block PEB-2.6/PEB-6.0/PEB-10.9/PEB-13.2 and a tri-block PEB-6.5/PEB-8.9/PEB-10.1, were synthesized via hydrogenation of poly(1,4-1,2) butadiene block random copolymer segments where the 1,4/1,2 ratio decreased as the number of segments increased. For example, the tetra-block material was prepared in cyclohexane using t-butyl-lithium as the initiator (at room temperature). The initial PEB-2.6 block was prepared with no modifier of the butadiene microstructure. On completion of the initial segment, a small amount of solution was removed for micro-structure (H-NMR) and chain molecular weight (H-NMR and GPC). The second segment was carried out with a small concentration of triethyl-amine present. This led to an enhanced vinyl concentration. After hydrogenation, this yielded the PEB-6.0 block. This procedure was repeated to prepare the subsequent PEB-10.9 and PEB-13.2 blocks (Radulescu et al. 2011). The measured averaged molecular weight of the two multi-block materials was 18.9kg mol^{-1} (6.3/6.3/6.3) for the tri-block and 29.7kg mol^{-1} (4.2/8.5/8.5/8.5) for the tetra-block, respectively.

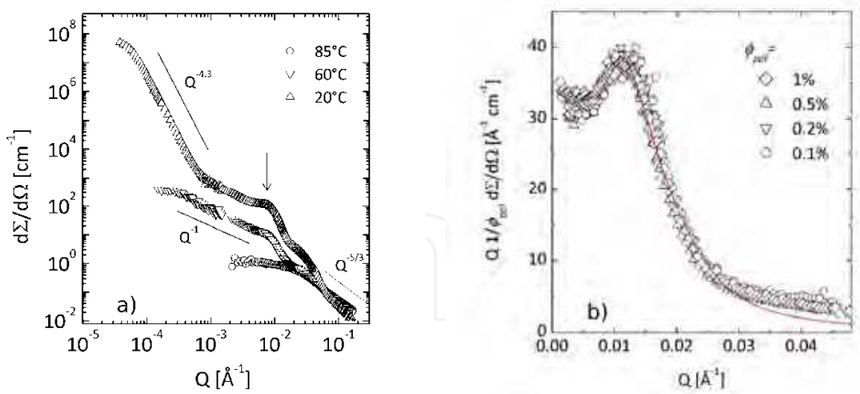

Fig. 16. (a) Selective examples of SANS patterns collected at several temperatures where typical structures are revealed in decane solution of 1% tetra-block copolymer (Radulescu et al., 2011); the power-law scattering behaviour characteristic of different structures is indicated; the arrow denotes the peak arising from intra-particle correlation as concluded following the observation of the constant peak-position for different ϕ_{pol} in solution, which is illustrated in (b) for the case of the tri-block copolymer in decane; the red curve represents the description of data with the density-modulated rod model.

A combination of classical pinhole-, mirror-focusing- and ultra-SANS techniques with microscopy (Radulescu et al., 2011) revealed that decreasing temperature leads to the formation and evolution in solution of multi-sized structural levels showing a hierarchical organization on the length scale from nanometres up to 10 of microns (Fig.16a). The tetra-block and tri-block copolymers show similar aggregation behaviour, and only the temperature at which the self-assembling commences is different for the two materials. This self-assembling behaviour relates to the graded crystallization tendency of the constituent blocks of copolymers upon cooling. In a first aggregation step, the scattering features at 60°C (Q^{-1} power law behaviour and the peak-like structure) revealed rod-like morphologies with modulated density formed as a consequence of the crystallization of the block containing the longer PE sequences following a mechanism described above in the case of PEB-*n* random copolymers. The nature of the aggregates and their structural characterization was established by model interpretation of the results from systematic pinhole-SANS investigations (Fig.16b). Subsequent crystallization events at lower temperature yield new structural features. On the one hand, micellar-like sub-structural morphologies arising from the amorphous segments anchored on growing correlated crystalline nuclei along the rod axis give raise to the occurrence in the scattering profile of a hump-like feature at Q=2-5x10^{-2} Å^{-1}. On the other hand, cross-linking of the one-dimensional aggregates due to co-crystallization of segments with lower crystallinity produced a dramatic increase of the scattered intensity towards low Q. Large-scale macro-aggregates with irregular edges and a diffusive interface (power-law exponent p>4) are ultimately formed as a consequence of these branching and association events. The understanding of the self-association mechanism was completed by the results of microscopy and contrast matching pinhole SANS on mixed solutions of multi-block copolymers and single waxes. These investigations helped elucidate the polymer-wax interaction mechanism at the microscopic level.

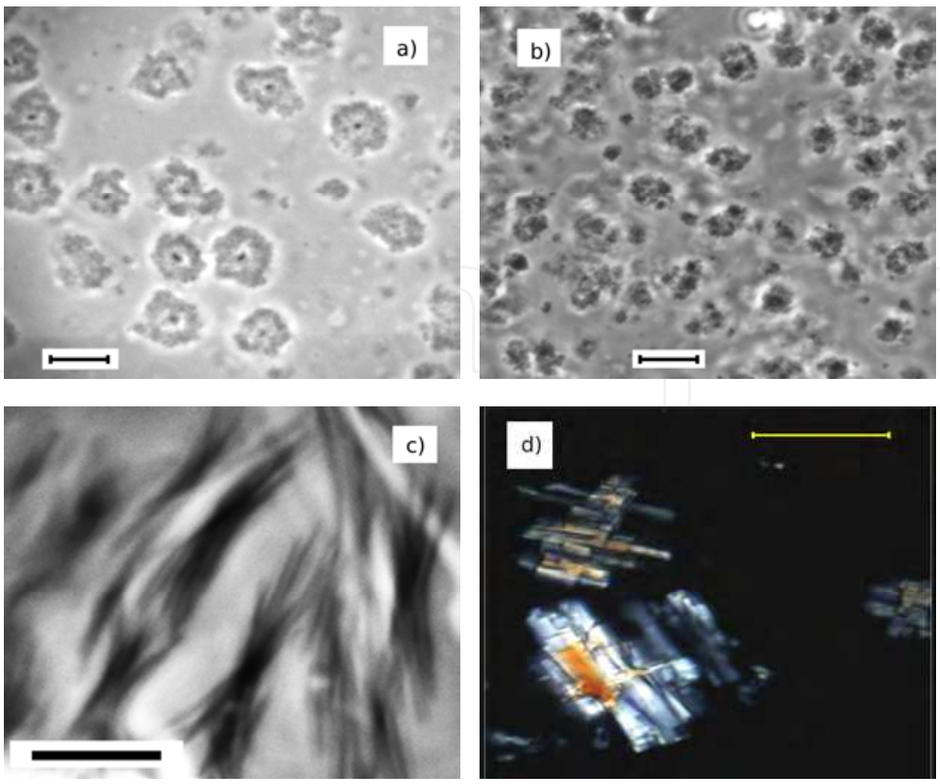

Fig. 17. Aggregates formed at 0°C in decane solution of 1% tetra-block copolymer with no wax (a), 1%C_{36} (b) and 4%C_{36} (c,d) added as revealed by bright field (a-c) and crossed polarizers (d) microscopy (Radulescu et al., 2011); the scale bar: 10μm (a-c), 20μm (d).

Polymer morphologies yielded by the gradual assembling behaviour are emphasized by decoration with wax crystallites (Fig.17b-d) when large wax-entrapping globular morphologies or sheaves and bundles of elongated wax crystals are observed under the microscope. For low wax content, the early formed polymer morphologies incorporate later appearing wax crystallites and hereby, they become more dense and compact. The limited growth of the polymer templates is an indication for less frequent branching events and thus, the incorporation of later crystallizing polymer segments within co-crystals with wax molecules. Fig.17c,d show bundles of fibrils and sheaves of elongated lamellae formed when the wax content is high. These crystal habits seem to be templated and controlled by polymers. After the analysis of systematic SANS data it turned out that the co-crystallization of the wax molecules and copolymers mid-branched crystallizing blocks is the key effect yielding the specific wax-copolymer morphology observed in this case (Radulescu et al., 2011). This emphasizes the specificity of the graded crystalline multi-block copolymers compared to the PEB-*n* random copolymers.

The formation of a primary structural level at certain temperatures is a consequence of crystallization occurring within the highly crystalline segment. Concurrently, cooling promotes a secondary structure which is anchored and hierarchically grows at the initial structure. In this way, the low temperature final morphology, although complex and multi-sized, exhibit smaller dimension and higher compactness compared to those yielded in the case of PEB-*n* random materials.

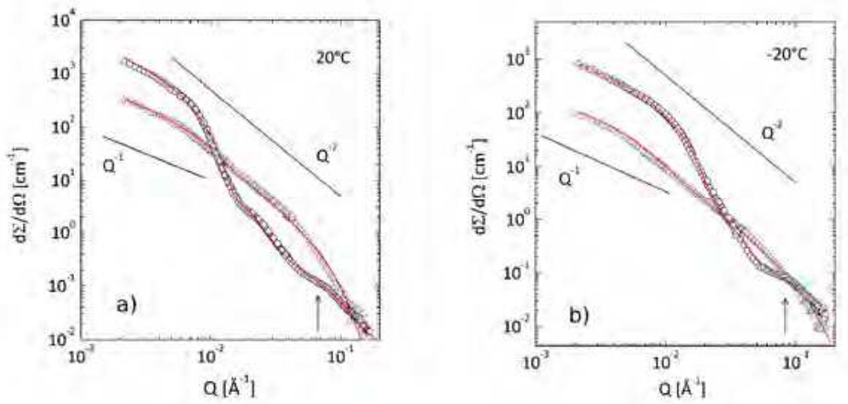

Fig. 18. Examples of SANS patterns measured from mixed 1%tetra-block/1%C_{36} (a) and 1%tri-block/1%C_{24} (b) decane solutions for the polymer (circles) and wax (triangles) visible; the red curves denote the model interpretation of data while the arrows indicate the high-Q scattering detail characteristic for polymer blobs.

The co-crystallization of wax and polymer from common solution in habits that are dictated by the polymer assembling tendency is revealed by a comparative analysis of contrast matched scattering patterns (Fig.18) and those measured from separate wax and polymer solutions (Fig.9, 16). On the one hand, the wax/copolymer common structures are templated by pre-existing polymer rod-like assemblies formed at higher temperatures than the wax crystallization point. This explains the overall one-dimensional morphology of the polymer and wax (Q^{-1} behaviour at low Q). On the other hand, according to the observed polymer scattering features (the disappearance of the intermediate-Q prominent peak and the preservation of the Q^{-1} power law), it seems that co-crystallizing wax and polymer molecules promote the growth of the initial polymer crystalline nuclei along the rod axis, filling eventually the open volume between them and generating more homogeneous aggregates. The polymer patterns were successfully modelled with the homogeneous rod form factor (Eq.8) with an added contribution of the scattering from polymer blobs describing the high Q modulation (Richter et al., 1997). The wax morphology seems to resemble thin and elongated platelets (boards) as revealed by the two characteristic power-laws (Q^{-1} at low Q and Q^{-2} at intermediate Q) and structural levels (kinks of intensity) observed in the scattering profile. The wax scattering patterns were rather well described by the form factor of very long cylinders with elliptical cross-section (Bergström & Pedersen, 1999), which is a good approximation for a tablet- or board-shaped morphology. Again, thin and very long crystals consisting of monolayer of elongated wax molecules and having a width of 500-600Å were revealed in both cases. The lesser extension of common wax-copolymer crystallization in the lateral direction together with the sign of polymer blobs formation is an evidence of aggregates consisting of rather compact very elongated core surrounded by amorphous polymer corona. The core is jointly made by wax and polymer whereas the corona that hinders the growth of the wax crystals into large compact three-dimensional objects consists of amorphous polymer segments. This explains why the correlation effect revealed by the scattering patterns from polymer self-assemblies vanishes in both the polymer and wax scattering patterns at temperatures under the wax

crystallization point and why the scattering features of the rods substructure also disappear in the polymer scattering profile. The PEB-*n* multi-block copolymers demonstrate high efficiency in reducing the size and in changing the shape of waxy crystals formed in single wax solutions. Board-like wax crystals that are basically formed (Fig.19) are entrapped by the polymer macro-aggregates or grow in a manner that is controlled by the polymer. The wax-polymer interaction mechanism deciphered with the help of micro-structural investigations is nicely emphasized in the case of high C_{36} wax containing solutions.

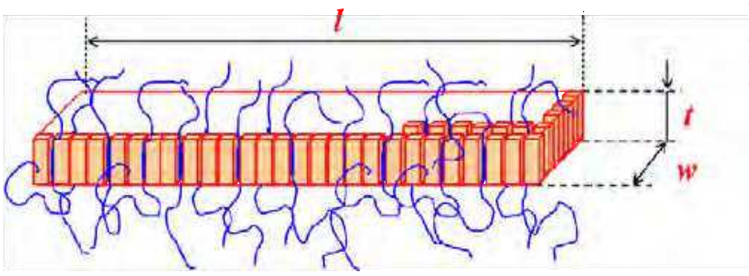

Fig. 19. Sketch depicting the wax board-like morphology controlled by the PEB-*n* multi-block copolymers emerged from the micro-structural studies; the main structural levels characterizing such morphology, the width *w*, the thickness *t*, and the length *l* are indicated.

The wax crystal control capacity of the multi-block PEB-*n* copolymers with graded crystallinity was further explored on more realistic systems with either high content of short *n*-paraffins (4% C_{24}) or mixture of long *n*-paraffin waxes (1%C_{30}+1%C_{36}), close to the conditions encountered in the oil industry applications. Fig.20a,b present the contrast matching SANS results from a 1%tri-block/4%C_{24} decane solution at two temperatures under the wax crystallization point. A co-crystallization of wax and polymer molecules in thin platelets (Q^{-2} power-law behaviour) is again the interaction mechanism revealed by the simultaneous interpretation of the polymer and scattering patterns collected at 0°C (Fig.20a). The plates seem to be weakly correlated as indicated by the broad hump-like feature observed in the wax profile. The modelling of data in terms of two wax and polymer embedded layers of different thickness proves that the wax crystals consist of single layer of stretched wax molecules while the form factor yields details of polymer structure. The analysis of the "forward scattering" resulted in a wax fraction included within the thin lamellar structures of about 15% from the total wax amount dissolved in the initial solution. This value is considerably higher than that obtained in the case of 1%PEB-7.5(6kg mol^{-1})/ 4%C_{24} at 0°C, which amounts to about 6%. A further decrease in temperature (Fig.20b) leaves the polymer conformation almost unchanged as observed in the scattering profile when compare to the 0°C case, but induces a dramatic changes at the level of wax morphology: although a certain amount of wax stays still in a two-dimensional conformation, as proven by the Q^{-2} power-law behaviour observed towards high *Q*, a massive growth of wax in large compact crystals is revealed by the Porod-like scattering observed at low *Q*.

The micrograph from the same sample (Fig.21a) shows the micron size compact aggregates that give rise to such scattering profile. Nevertheless, when compared with the case of the neat wax solution (Fig.8d) the wax crystal control ability of the multi-blocks is striking. The polymer seems to operate by a two-fold mechanism: on one hand, it templates the wax

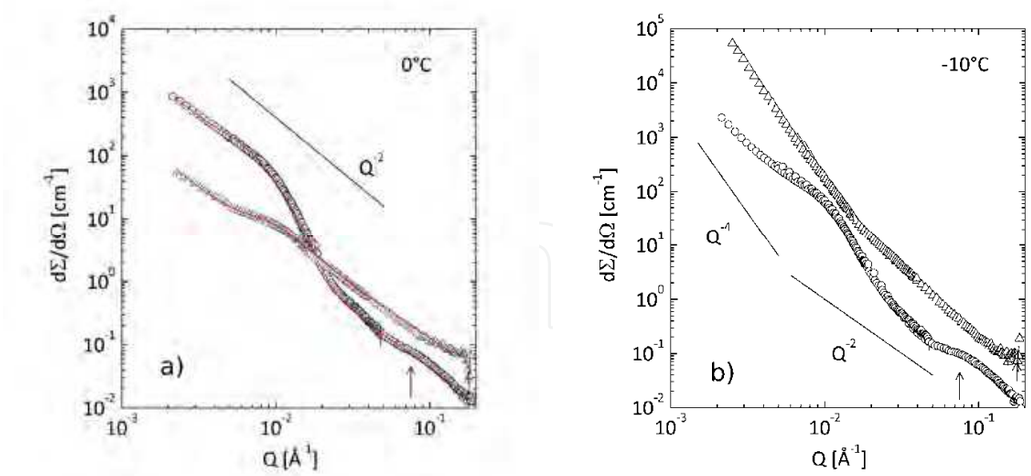

Fig. 20. Examples of contrast matched polymer (circles) and wax (triangles) scattering patterns from 1%tri-block/4%C_{24} decane solution at two different temperatures. The curves and arrows have the same meaning as in Fig.18.

crystallization by means of its early formed primary morphology and, on the other hand, it arrests the growth of large wax crystals by a moderate co-crystallization of wax molecules and mid-branched segments entrapped by the still amorphous segments.

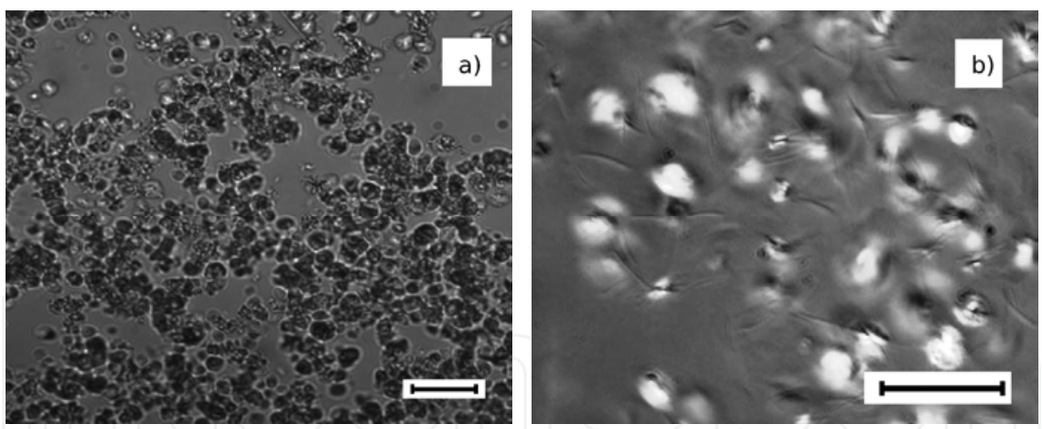

Fig. 21. Micrographs from decane solutions of 1% tri-block and 4%C_{24} at -10°C (a) and 1% tetra-block and 1%C_{30}+1%C_{36} at 0°C; scale bars are 30μm.

In the case of tetra-blocks added to a mixed 1%C_{30}+1%C_{36} decane solution the micrographs collected at 0°C (Fig.21b) also revealed the formation of very small morphologies which differs greatly from the case of polymer undoped solution (Fig.8a). The SANS scattering patterns collected for wax contrast (Fig.22a) show that most of wax stays in a two-dimensional morphology at 10°C and 0°C, under the crystallization point of the two wax molecules. A moderate increasing tendency of the scattered intensity towards low Q with a power law exponent $p \approx 3$ is evident at 0°C when wax-driven agglomerates showing irregular rough edges are formed.

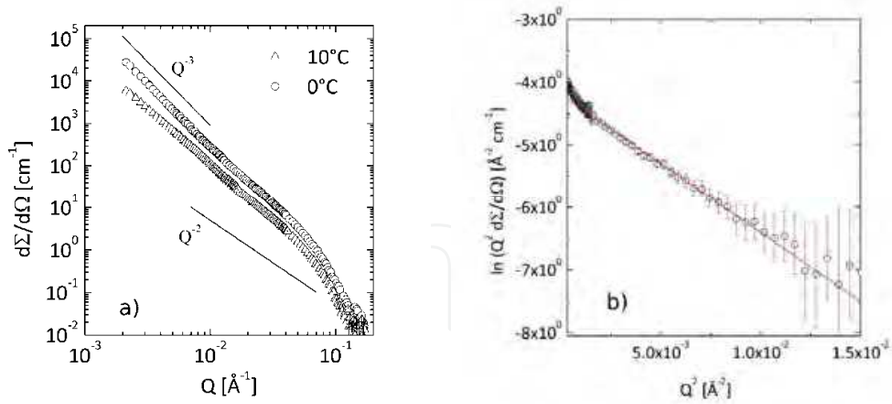

Fig. 22. SANS patterns under wax contrast from a 1% tetra-block and 1%C_{30}+1%C_{36} solution in decane (a) and the Guinier presentation of the large *Q* data at 0°C, delivering in a direct approach the thickness and the "forward scattering" of the wax lamellae (b).

A close inspection of the micrograph shows besides these aggregates some other elongated objects resembling the one-dimensional crystals observed in the case of tetra-block and single C_{36} wax. These fibrillar-shaped crystals seem to be dominantly wax containing, as in the case of large C_{36} content (Fig.17c), while the larger irregular morphologies must result from waxes entrapped by polymer branched aggregates. A quick quantitative analysis of data in a two-dimensional Guinier approach (Fig.22b) delivered the "forward scattering" from the thin wax layers which revealed that about 50% from the total amount of wax dissolved in the initial solution is contained by the two-dimensional morphologies at 0°C, which again proves the efficiency of these polymers in controlling the wax crystallization from hydrocarbon solutions.

7. Concluding remarks

Hopefully, in this work we have demonstrated the uniqueness and usefulness of small-angle neutron scattering to solve and characterize the complex morphologies formed in common solutions of *n*-paraffin waxes and polymeric systems upon decreasing temperature and, based on the contrast matching method and with the support of the complementary microscopy approach, to understand the subtleties of wax-polymer interaction mechanism at a mesoscopic scale. The elucidation and the knowledge of fundamental aspects concerning the structures and morphologies emerging in such systems as a function of temperature, concentration in solution and, more important, similarities in the assembling and crystallization behaviour between the two systems of interest, namely the wax and the polymer, can lead to direct predictions and immediate applicability with respect to the wax crystal control capacity of distinct polymeric systems. Thus, highly efficient polymer additives can be tailored for acting against specific technical problems experienced by the oil and refinery industry as a consequence of the cold wax crystallization depending on particularities of the systems and conditions involved. As a general conclusion, polymeric systems presenting graded crystallinity have proven a high efficacy and versatility in controlling the crystallization of waxes in various conditions.

8. References

Abdallah, D.J. & Weiss, R.G. (2000). n-Alkanes Gel n-Alkanes (and many other organic liquids). *Langmuir*, Vol.16, No.2, pp.352-355, ISSN 0743-7463

Alefeld, B.; Dohmen, L.; Richter, D. & Brückel, T. (2000). X-Ray Space Technology for Focusing Small-Angle Neutron Scattering and Neutron Reflectometry. *Physica B*, Vol.283, No.4, pp.330-332, ISSN 0921-4526

Ashbaugh, H.S.; Radulescu, A.; Prud'homme, R.K.; Schwahn, D.; Richter, D. & Fetters, L.J. (2002). Interaction of Paraffin Wax Gels with Random Crystalline/Amorphous Hydrocarbon Copolymers. *Macromolecules*, Vol.35, No.18, pp.7044-7053, ISSN 0024-9297

Banki, R.; Hoteit, H. & Firoozabadi, A. (2008). Mathematical Formulation and Numerical Modeling of Wax Deposition in Pipelines from Enthalpy-Porosity Approach and Irreversible Thermodynamics. *International Journal of Heat Mass Transfer*, Vol.51, No.13-14, pp.3387-3398, ISSN 0017-9310

Beaucage, G. & Schaefer, D.W. (1994). Structural Studies of Complex-Systems Using Small-Angle Scattering – A Unified Guinier Power-Law Approach. *Journal of Non-Crystalline Solids*, Vol.172-174, pp.797-805, ISSN 0022-3093

Beiny, D.H.M.; Mulli, J.W. & Lewtas, K. (1990). Crystallization of Normal-Dotriacontane from Hydrocarbon Solution with Polymeric Additives. *Journal of Crystal Growth*, Vol.102, No.4, pp.801-806, ISSN 0022-0248

Bergström, M. & Pedersen, J.S. (1999). A Small-Angle Neutron Scattering (SANS) Study of Tablet-Shaped and Ribbonlike Micelles Formed from Mixtures of an Anionic and a Cationic Surfactant. *Journal of Physical Chemistry B*, Vol.103, No.40, pp.8502-8513, ISSN 1089-5647

Claudy, P.; Letoffe, J.M.; Bonardi, B.; Vassilakis, D. Damin, B. (1993). Interactions between n-Alkanes and Cloud Point-Cold Filter Plugging Point Depressants in a Diesel Fuel. A Thermodynamic Study. *Fuel*, Vol.72, No.6, pp.821-827, ISSN 0016-2361

Coutinho, J.A.P.; Dauphin, C. & Daridon J.L. (2000). Measurements and Modelling of Wax Formation in Diesel Fuels. *Fuel*, Vol.79, No.6, pp.607-616, ISSN 0016-2361

del Carmen Garcia, M.; Carbognani, L.; Orea, M. & Urbina A. (2000). The Influence of Alkane Class-Type on Crude Oil Wax Crystallization and Inhibitors Efficiency. *Journal of Petroleum Science and Engineering*, Vol.25, No.3-4,pp.99-105, ISSN 0920-4105

Frielinghaus, H.; Pipich, V.; Radulescu, A.; Heiderich, M.; Hanslick, R.; Dahlhoff, K.; Iwase, H.; Koizumi, S. & Schwahn, D. (2009). Aspherical Refractive Lenses for Small-Angle Neutron Scattering. *Journal of Applied Crystallography*, Vol.42, No.4, pp.681-690, ISSN 0021-8898

Giorgio, S. & Kern, R. (1983). Filterability, Crystal Morphology and Texture – Paraffin Dewaxing Aids. *Journal of Crystal Growth*, Vol.62, No.2, pp.360-374, ISSN 0022-0248

Kern, R. & Dassonville, R. (1992). Growth Inhibitors and Promoters Exemplified on solutionj Growth of Paraffin Crystals. *Journal of Crystal Growth*, Vol.116, No.1-2, pp.191-203, ISSN 0022-0248

Leube, W.; Monkenbusch, M.; Schneiders, D.; Richter, D.; Adamson, D.; Fetters, L. & Dounis, P. (2000). Wax-Crystal Modification for Fuel Oils by Self-Aggregating Partially Crystallizable Hydrocarbon Block-Copolymers. *Energy Fuels*, Vol.14. No.2, pp.419-430, ISSN 0887-0624

Monkenbusch, M.; Schneiders, D.; Richter, D.; Willner, L.; Leube, W.; Fetters, L.J.: Huang, J.S. and Lin, M. (2000). Aggregation Behaviour of PE-PEP Copolymers and the Winterization of Diesel Fuel. *Physica B*, Vol.276-278, pp.941-943, ISSN 0921-4526

Morton, M. & Fetters, L.J. (1975). Anionic Polymerization of Vinyl Monomers. *Rubber Chemistry and Technology*, Vol.48, No.3, pp.359-409, ISSN 0035-9475

Pedersen, J.S. (1997). Analysis of Small-Angle Scattering Data from Colloids and Polymer Solutions: Modelling and Least-Square Fitting. *Advances in Colloid and Interface Science*, Vol.70, No.,pp.171-210, ISSN 0001-8686

Pedersen, K.S.; Skovbor, P. and Ronningsen H.P. (1991a). Wax Precipitation from North Sea Crude Oils. 4. Thermodynamic Modelling. *Energy Fuels*, Vol.5, No.6, pp.924-932, ISSN 0887-0624

Pedersen, W.B.; Hansen, A.B.; Larsen, E.; Nielsen, A.B. and Ronningsen, H.P. (1991b). Wax Precipitation from North Sea Crude Oils. 2. Solid-Phase Content as a Function of Temperature. *Energy Fuels*, Vol.5, No.6, pp.908-913, ISSN 0887-0624

Radulescu, A.; Schwahn, D.; Richter, D. & Fetters, L.J. (2003). Co-Crystallization of Poly(Ethylene-Butene) Copolymers and Paraffin Molecules in Decane Studied with Small-Angle Neutron Scattering. *Journal of Applied Crystallography*, Vol.36, No.4, pp.995-999, ISSN 0021-8898

Radulescu, A.; Schwahn, D.; Monkenbusch, M.; Fetters, L.J. & Richter, D. (2004). Structural Study of the Influence of Partially Crystalline Poly(Ethylene Butene) Random Copolymers on Paraffin Crystallization in Dilute solutions. *Journal of Polymer Science Part B – Polymer Physics*, Vol.42, No.17, pp.3113-3132, ISSN 0887-6266

Radulescu, A.; Schwahn, D.; Stellbrink, J., Kentzinger, E.; Heiderich, M.; Richter, D. & Fetters, L.J. (2006). Wax Crystallization from Solution in Hierarchical Morphology Templated by Random Poly(Ethylene-co-Butene) Self-Assemblies. *Macromolecules*, Vol.39, No.18, pp.6142-6151, ISSN 0024-9297

Radulescu, A.; Fetters, L.J. & Richter, D. (2008). Polymer-Driven Wax Crystal Control Using Partially Crystalline Polymeric Materials. *Advances in Polymer Science*, Vol.210, pp.1-100, ISSN 0065-3195

Radulescu, A.; Schwahn, D.; Stellbrink, J.; Monkenbusch, M.; Fetters, L.J. & Richter, D. (2011). Microstructure and Morphology of Self-Assembling Multiblock Poly(Ethylene-1-Butene)-n Copolymers in solution Studied by wide-Q Small-Angle Neutron Scattering and Microscopy. *Journal of Polymer Science Part B – Polymer Physics*, Vol.49, No.2, pp.144-158, ISSN 0887-6266

Richter, D.; Schneiders, D.; Monkenbusch, M.; Willner, L.; Fetters, L.J.; Huang, J.S.; Lin, M.; Mortensen, K. & Farago, B. (1997). Polymer Aggregates with Crystalline Cores: the System Poly-Ethylene-Poly(Ethylenepropylene). *Macromolecules*, Vol.30, No.4, pp.1053-1068, ISSN 0024-9297

Schwahn, D.; Richter, D., Wright, P.J.; Symon, C.; Fetters, L.J. & Lin, M. (2002a). Self-Assembling Behaviour in Decane Solution of Potential Wax Crystal Nucleators Based on Poly(co-Olefins). *Macromolecules*, Vol.35, No.3, pp.861-870, ISSN 0024-9297

Schwahn, D.; Richter, D.; Lin, M. & Fetters, L.J. (2002b). Cocrystallization of a Poly(Ethylene-Butene) Random Copolymer with C-24 in n-Decane. *Macromolecules*, Vol.35, No.9, pp.3762-3768, ISSN 0024-9297

Singh, P.; Fogler, H.S. & Nagarajan N. (1999). Prediction of the Wax Content of the Incipient Wax-Oil Gel in a Pipeline: an Application of the controlled Stress Rheometer. *Journal of Rheology*, Vol.43, No.6, pp.1437-1459, ISSN 0148-6055

Srivastava, S.P.; Saxena, A.K.; Tandon, R.S. & Shekher, V. (1997). The Measurement and Description of the Yielding Behavior of Waxy Crude Oil. *Fuel*, Vol.35, No.7, pp.1121-1156, ISSN 0016-2361

Venkatesan, R.; Nagarajan, N.R.; Paso, K.; Yi, Y.B.; Sastray, A.M. & Fogler H.S. (2005). The Strength of Paraffin Gels Formed Tinder Static and Flow Conditions. *Chemical Engineering Science*, Vol.60, No.13, pp.3587-3598, ISSN 0009-2509

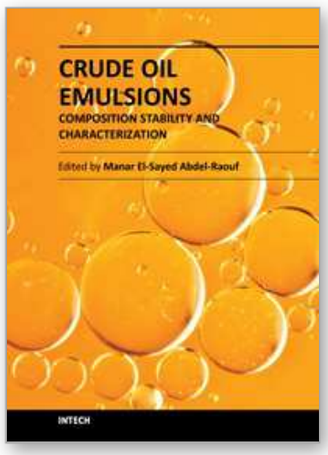

Crude Oil Emulsions- Composition Stability and Characterization

Edited by Prof. Manar El-Sayed Abdul-Raouf

ISBN 978-953-51-0220-5
Hard cover, 230 pages
Publisher InTech
Published online 02, March, 2012
Published in print edition March, 2012

Petroleum "black gold" is the most important nonrenewable source of energy. It is a complex mixture of different phases and components. Refining it provides a vast number of organic compounds, all of them of which are used to produce petroleum based products for numerous applications, from industry to medicine, from clothing to food industries. We can find petroleum based products all around us. This book deals with some important topics related to petroleum such as its chemical composition and stability. It is well-known that the chemical composition of crude oil differs according to the site of production, and its grade varies from waxy to asphaltenic crude. Both of them are refined to produce different products. The stability of crude oil on aging and transportation is governed by several factors and these factors are included within this book. Some new technologies for petroleum characterization are also introduced. This book is aimed at researchers, chemical engineers and people working within the petroleum industry.

How to reference

In order to correctly reference this scholarly work, feel free to copy and paste the following:

Aurel Radulescu, Lewis J. Fetters and Dieter Richter (2012). Tailored Polymer Additives for Wax (Paraffin) Crystal Control, Crude Oil Emulsions- Composition Stability and Characterization, Prof. Manar El-Sayed Abdul-Raouf (Ed.), ISBN: 978-953-51-0220-5, InTech, Available from: http://www.intechopen.com/books/crude-oil-emulsions-composition-stability-and-characterization/tailored-polymer-additives-for-wax-paraffin-crystal-control

INTECH
open science | open minds

InTech Europe
University Campus STeP Ri
Slavka Krautzeka 83/A
51000 Rijeka, Croatia
Phone: +385 (51) 770 447
Fax: +385 (51) 686 166
www.intechopen.com

InTech China
Unit 405, Office Block, Hotel Equatorial Shanghai
No.65, Yan An Road (West), Shanghai, 200040, China
中国上海市延安西路65号上海国际贵都大饭店办公楼405单元
Phone: +86-21-62489820
Fax: +86-21-62489821

IntechOpen